Phycobilins as Potent Food Bioactive Broad-Spectrum Inhibitors Against Proteases of SARS-CoV-2 and Other Coronaviruses: A Preliminary Study

Brahmaiah Pendyala[1]*, Ankit Patras[1]* and Chandravanu Dash[2]

[1] Department of Agricultural and Environmental Sciences, Food Science Program, College of Agriculture, Tennessee State University, Nashville, TN, United States, [2] Meharry Medical College, Nashville, TN, United States

In the 21st century, we have witnessed three coronavirus outbreaks: SARS in 2003, MERS in 2012, and the ongoing pandemic coronavirus disease 2019 (COVID-19). The search for efficient vaccines and development and repurposing of therapeutic drugs are the major approaches in the COVID-19 pandemic research area. There are concerns about the evolution of mutant strains (e.g., VUI – 202012/01, a mutant coronavirus in the United Kingdom), which can potentially reduce the impact of the current vaccine and therapeutic drug development trials. One promising approach to counter the mutant strains is the "development of effective broad-spectrum antiviral drugs" against coronaviruses. This study scientifically investigates potent food bioactive broad-spectrum antiviral compounds by targeting main protease (M^{pro}) and papain-like protease (PL^{pro}) proteases of coronaviruses (CoVs) using *in silico* and *in vitro* approaches. The results reveal that phycocyanobilin (PCB) shows potential inhibitor activity against both proteases. PCB had the best binding affinity to Mpro and PLpro with IC_{50} values of 71 and 62 μm, respectively. Also, *in silico* studies with M^{pro} and PL^{pro} enzymes of other human and animal CoVs indicate broad-spectrum inhibitor activity of the PCB. As with PCB, other phycobilins, such as phycourobilin (PUB), phycoerythrobilin (PEB), and phycoviolobilin (PVB) show similar binding affinity to SARS-CoV-2 M^{pro} and PL^{pro}.

Keywords: food bioactive constituents, broad-spectrum inhibitors, coronaviruses, SARS-CoV-2, COVID-19, main protease, papain-like protease

INTRODUCTION

Coronaviruses (CoVs) belongs to the subfamily of Orthocoronavirinae, family Coronavidae, order Nidovirales. They are large (average diameter of 120 nm), enveloped, positive-sense single-stranded RNA viruses with a genome size of ~26 to 32 kb (Woo et al., 2010). Based on antigen cross-reactivity and genetic makeup, four subgroups (alpha, beta, gamma, and delta) are subdivided into 26 different species of CoVs (Cleri et al., 2010). CoVs cause diseases in mammals and birds; alpha and beta group CoVs are pathogenic to humans (Paules et al., 2020). The seven CoVs that can cause

infectious diseases in humans are HCoV-229E, HCoV-NL63, HCoV-OC43, HCoV-HKU1, severe acute respiratory syndrome coronavirus (SARS-CoV), Middle East respiratory virus coronavirus (MERS-CoV), and 2019-nCoV (2019-novel coronavirus) or SARS-CoV-2 (Hamre and Procknow, 1966; McIntosh et al., 1967; Drosten et al., 2003; van der Hoek et al., 2004; Woo et al., 2005; Bermingham et al., 2012; Wu F. et al., 2020). The first four common CoVs persistently circulate in humans and are responsible for 10–30% of common colds (Paules et al., 2020). The other three deadly viruses are etiological agents of fatal respiratory syndromes SARS, MERS, and coronavirus disease 2019 (COVID-19), respectively. The SARS epidemic in 2003 ended with 8098 reported cases, 774 deaths (fatality rate 9.7%), whereas the MERS outbreak in 2012 caused 2494 reported cases, 858 deaths (fatality rate 34%) (World Health Organization (WHO), 2003; Alfaraj et al., 2019). COVID-19, the current pandemic outbreak, first identified in 2019, report >37.1 million confirmed cases with >1.07 million deaths (fatality rate 2.9%) as of October 12, 2020 (World Health Organization (WHO), 2020). Avian infectious bronchitis virus (IBV), feline infectious peritonitis virus (FIPV), canine CoV, and porcine transmissible gastroenteritis virus (TGEV) cause respiratory and enteric diseases in farm and domestic pet animals (Pratelli, 2006; Cavanagh, 2007; Pedersen, 2009; Odend'hal, 2012).

Till now, there are no approved vaccines and therapeutic drugs for COVID-19 or other human coronavirus infections and a lack of enough clinical trial data to make treatment decisions. Although vaccines have been developed against animal viruses IBV, canine CoV, and TGEV to help prevent serious diseases (Park et al., 1998; Carmichael, 1999; Liu and Kong, 2004), there are some potential problems, such as recombination events between field and vaccine strains, the emergence of novel serotypes, and antibody-dependent enhancement remain. The rapid development of vaccines and repurposing of approved antivirals drugs (e.g., remdesivir) are major clinical approaches of a pandemic preparedness plan. The development of broad-spectrum antiviral agents that are effective against a wide range of CoVs and other classes of viruses, including emerging ones, could be a promising strategy (Bekerman and Einav, 2015; Fauci and Morens, 2016; Cho and Glenn, 2020).

Broad-spectrum antiviral targeting strategies can be classified into two categories: (i) entry inhibitors that interact with existing virus particles outside of cells and prevent infection (Hangartner et al., 2006) and (ii) replication inhibitors aimed at stopping viral genome replication to curtail production of new virus particles (De Clercq, 2004). The S glycoprotein of coronaviruses, the main determinant of host cell attachment and viral entry, is not well conserved between HCoVs (Totura and Bavari, 2019). On the other hand, CoV non-structural proteins (nsps) are highly conserved components of the coronavirus life cycle that mediate viral replication (Totura and Bavari, 2019). Literature studies report the following SARS-CoV-2 nsp targets; main protease (M^{pro}), papain-like protease (PL^{pro}), Nsp3, RdRp, Helicase, Nsp14, Nsp15, Nsp16, N protein to inhibit virus replication (Wu C. et al., 2020). Proteolytic processing of viral polyproteins into functional nsps by two viral proteases, the M^{pro} and PL^{pro}, is an important event of the CoV life cycle. The M^{pro} acts on minimum

11 cleavage sites of replicase 1ab, ~790 kDa; at recognition sequence Leu-Gln↓ (Ser, Ala, Gly) (↓ indicates cleavage site), most cleavage sites block viral replication (Zhang et al., 2020). PL^{pro} enzyme hydrolyses the peptide bond at the carboxyl side of glycine (P1 position) and releases nsp1, nsp2, and nsp3 functional proteins, which play a key role in viral replication (Rut et al., 2020). Therefore, these proteases would be potential targets for the development of broad-spectrum antiviral drugs. CoVs M^{pro} and PL^{pro} crystal structures are available for public access in the protein data bank (PDB).

Natural food bioactive compounds are gaining importance as supplementary antiviral therapeutic compounds in the modern healthcare sector because of their lower toxicity and fewer side effects, additional health benefits (antioxidant, anti-inflammatory, and immunomodulation activities), and potential use in conjunction with preexisting therapies. Several literature studies report antiviral properties of food bioactive compounds against CoVs and other viruses (**Table 1**; Ghildiyal et al., 2020; Mani et al., 2020). In view of the issues posed above, identifying natural food bioactive broad-spectrum antiviral agents against the CoVs is a more reasonable and attractive prospect and could provide an effective first line of defense against future emerging CoVs related diseases. Herein, we report the phycobilins as potent food bioactive broad-spectrum inhibitor compounds against M^{pro} and PL^{pro} of SARS-CoV-2 and other CoVs via *in silico* and *in vitro* approaches.

MATERIALS AND METHODS

In silico Screening of Inhibitor Compounds

Preparation of Protein and Ligand for Docking

The crystal structures of M^{pro} (PDB ID – 6LU7) and PL^{pro} of SARS-CoV-2 (PDB ID – 6WUU) and other CoVs used in this study were obtained from the RCSB PDB. Ligand structures were obtained from Pubchem and Chemical Entities of Biological Interest (ChEBI) as SDF format, Open Babel was used for format transformation or 3-D coordinate generation for the uploaded files (O'Boyle et al., 2011). The MGLTools were used to delete other chains, and heteroatoms (included water), adding missing atoms, hydrogens, and charges. Further, the pdbqt files were prepared for proteins and ligands binding.

Molecular Docking and Molecular Simulation Studies

Autodock Vina was used as a docking engine. It is critical to define the docking grid box appropriately due to the small molecule docking procedure (Trott and Olson, 2010). The docking box is defined as the center of native ligand coordinates with 40 Å × 40 Å × 40 Å in length to include the residues of the entire cavity, and the exhaustiveness level was set on 12 with number of modes 10. For visualization, the docking results PDBQT files were exported, and docked protein-ligand complex structures were visualized using Pymol. Active site residues within 3 or 3.5 Å of ligand and polar contacts were determined with this same tool. The ligand docking procedure was validated by redocking of the native

TABLE 1 | Antiviral properties of selected food bioactive constituents.

Bioactive compound	Antiviral activity	References
Phycocyanobilin	Spirulina extract exhibited anti-flu efficacy against wide range of influenza viruses with EC_{50} values from 0.58 to 1.17 mg/mL.	Chen et al., 2016
Quercetin	Inhibited hepatitis C virus production almost completely (>95%) at concentration of 10 μM.	Bachmetov et al., 2012
Riboflavin	In combination with poly r(A-U) showed 7 to 12-fold antiviral activity against human foreskin fibroblast-vesicular stomatitis virus	Jamison et al., 1990
Cyanidin	Cyanidin-3-sambubiocide was found to be a potent inhibitor for H1N1 neuraminidase (NA) activity with IC_{50} value 72 μM.	Kannan and Kolandaivel, 2018
Daidzein	Exhibited anti-dengue activity with $IC_{50} = 142.6$ μg mL^{-1} against DENV-2.	Zandi et al., 2011
Genistein	Reduced hepatitis B virus production with an IC_{50} value of 33 and 46 μM for human and macaque fibroblasts, respectively.	LeCher et al., 2019
Catechin	Catechins (−)-epigallocatechin gallate (EGCG), (−)-epicatechin gallate (ECG) were identified as potent inhibitors of influenza virus replication with EC_{50} of 22–28 and 22–40 μM, respectively.	Song et al., 2005
Resveratrol	MERS-CoV titer reduced 4 logs by resveratrol treatment at 250 μM concentration after 48 h of infection.	Lin et al., 2017
Curcumin	Curcumin and its derivatives showed antiviral effects on HSV-1 in cell culture with IC_{50} values in range of 13.9–33.0 μg/mL.	Zandi et al., 2010
Astaxanthin	Pre-treatment of Vero cells with 75 μg mL^{-1} of *Haematococcus pluvialis* ethanol extract with carotenoids inhibited Herpes simplex virus type 1 (HSV-1) infection by approximately 85%.	Santoyo et al., 2012
β-carotene	Pre-treatment of Vero cells with 75 μg mL-1 of *H. pluvialis* ethanol extract with carotenoids inhibited Herpes simplex virus type 1 (HSV-1) infection by approximately 85%.	Santoyo et al., 2012
Capsaicin	Methanolic extract of *Capsicum annuum* exhibited a considerable anti-HSV-1 and anti-HSV-2 activities at the concentration of 25 μg/mL.	Hafiz et al., 2017
Gingerol	Fresh *Zingiber officinale* inhibited human respiratory syncytial virus (HRSV) with IC_{50} of 144.9 μg/mL in HEp-2 cells and 73.3 μg/ml in A549 cells.	San Chang et al., 2013
Vanillin	MY21 (a vanillin derivative) had the IC_{50} of 50 μM against H1N1 neuraminidase (NA).	Hariono et al., 2016
Eugenol	IC_{50} values for the anti-HSV effects of eugenol were 25.6 and 16.2 μg/mL for HSV-1 and HSV-2, respectively.	Benencia and Courreges, 2000
Thymol	Exhibited significant antiviral activity with an IC50 of 7 μM against herpes simplex virus type I.	Lai et al., 2012

ligand with the same protocol and the grid parameters as used for food bioactive compounds. The redocked ligand was then superimposed onto the reference co-crystallized ligand

complex using Pymol, and the root mean square deviation (RMSD) was analyzed.

Molecular dynamic simulations were performed using NAMD (Phillips et al., 2005). The parameters, structure, and topology files for the ligand were generated using the CHARMM-GUI Web server (Jo et al., 2008). Visual molecular dynamics (VMD) was used to generate protein structure (PSF) files (Humphrey et al., 1996). Each protein-ligand docked complex was solvated and ionized with 0.15 M ions (Na+ and Cl−) to neutralize the charge and electrostatic screening. The systems were subjected to 2000 steps of steepest descent energy minimization before a production run at the NPT of 0.5 ns (250,000 steps). The temperature (310 K) and pressure (1 atm) were controlled by the Langevin and Langevin piston methods (Feller et al., 1995). VMD software was used to visualize simulations and to analyze average ligand-RMSD and protein-RMSD and hydrogen bonds.

In vitro Enzymatic Assays

For enzyme inhibition studies, selected phytochemicals, PCB, Quercetin, Riboflavin, Cyanidin, Daidzein, and Genistein, were purchased from Santa Cruz Biotechnology (Santa Cruz, CA, United States). Enzyme assay kits, 3CL Protease, MBP-tagged (SARS-CoV-2) assay (Catalog #79955), and papain-like protease (SARS-CoV-2) assay kit: protease activity (Catalog #79995), were purchased from BPS Bioscience (San Diego, CA, United States).

M^{pro} Assay

Fluorescence resonance energy transfer (FRET)-based cleavage assay (Zhu et al., 2011) was used for *in vitro* enzyme inhibition study. SARS-CoV-2 M^{pro} or 3CL Protease, GenBank Accession No. YP_009725301, amino acids 1-306 (full length), with an N-terminal MBP-tag, expressed in an *Escherichia coli* and its fluorescent substrate with cleavage site (indicated by ↓) DABCYL-KTSAVLQ↓SGFRKME-EDANS, inhibitor control (GC376), and the assay buffer composed of 20 mM Tris, 100 mM NaCl, 1 mM EDTA, 1 mM DTT, pH 7.3 were used. Initially, 15 μL of the SARS-CoV-2 M^{pro} in reaction buffer at the final concentration of 10 ng/μL and 5 μL of inhibitor control (GC376, final concentration 50 μM)/test inhibitor (10–600 μM)/inhibitor solvent (positive control) was pipetted into a 384-well plate. Stock solutions of the compounds were prepared with 100% DMSO. Afterward, the plate was preincubated for 30 min at room temperature with slow shaking. The enzymatic reaction was then initiated by adding of 5 μL of the substrate dissolved in the reaction buffer to 25 μL final volume (final concentration 50 μM) and incubated at room temperature for 4 h. The fluorescence signal of the Edans generated due to the cleavage of the substrate by the M^{pro} was monitored at excitation at 360 nm with an emission wavelength of 460 nm, using a spectrophotometric microplate reader (Synergy H1 Hybrid Multi-Mode Reader; BioTek Instruments, Inc., Winooski, VT, United States).

PL^{pro} Assay

Severe acute respiratory syndrome coronavirus-2 PL^{pro} (papain-like protease), GenBank Accession No. QHD43415, amino acids 1564–1882, with N-terminal His-tag, expressed in an *E. coli* and its fluorescent substrate Z-Arg-Leu-Arg-Gly-Gly-AMC, inhibitor

control (GRL0617) and the assay buffer (40 mM Tris pH 8, 110 mM NaCl, 1 mM DTT) was used for the inhibition assay. Briefly, 30 μL of the SARS-CoV-2 PL^{pro} in reaction buffer at the final concentration of 0.44 ng/μL and 10 μL of inhibitor control (GRL0617, final concentration 100 μM)/test inhibitor (10–600 μM)/inhibitor solvent (positive control) was pipetted into a 96-well plate. Afterward, the plate was preincubated for 30 min at room temperature with slow shaking. The enzymatic reaction was then initiated by the addition of 10 μL of the substrate dissolved in the reaction buffer to 50 μL final volume (final concentration 25 μM), incubated at room temperature for 40–60 min. The fluorescence signal of the substrate after the enzymatic reaction was monitored at an excitation at 360 nm with an emission wavelength of 460 nm, using a spectrophotometric microplate reader (Synergy H1 Hybrid Multi-Mode Reader; BioTek Instruments, Inc., Winooski, VT, United States). Triplicate experiments ($N = 3$) were performed for both M^{pro} and PL^{pro} assays, and the mean value was presented with ± standard deviation (SD).

RESULTS

Selection of Phytochemicals for the Study

A total of 16 phytochemicals from different chemical classes were selected based on the previous reports of their potent antiviral effects (**Table 1**): linear tetrapyrrole – phycocyanobilin (PCB), flavonols – quercetin, catechin, flavin – riboflavin, anthocyanin – cyanidin, isoflavones – daidzein, genistein, stilbenoid phenol – resveratrol, linear diarylheptanoid – curcumin, Xanthophyll – astaxanthin, carotenes – β-carotene, phenolic alkaloid – capsaicin, phenolic ketone – gingerol, phenolic

aldehyde – vanillin, allylbenzene – eugenol, monoterpenoid phenol – thymol.

In silico Binding Interaction Studies of Selected Phytochemical Compounds With SARS-CoV-2 M^{pro} and PL^{pro}

The 16 selected phytochemicals were docked into the active site pocket of SARS-CoV-2 M^{pro} and PL^{pro}. **Table 2** depicts the source, docking score, and polar contacts of selected phytochemical bioactive compounds with binding site amino acid residues of SARS-CoV-2 proteases. For M^{pro}, the results show PCB docked with the best score or binding energy of −8.6 Kcal/mol followed by Riboflavin (−7.9 Kcal/mol), Cyanidin (−7.9 Kcal/mol), Daidzein (−7.8 Kcal/mol), and Genistein (−7.6 Kcal/mol). Twelve key active-site amino acid residues (Tyr 54, Gly 143, His 163, Asp 187, Gln 189, Glu 166, Cys 145, Leu 141, Ser 144, Thr 26, Gln 192, and Thr 190) of SARS-CoV-2 M^{pro} involved in polar interactions at a distance of ≤3 Å with ligand phytochemical compounds. Specific polar contacts of each phytochemical compound are shown in **Table 2**. In the case of PL^{pro}, as the reported peptide inhibitor VIR250 is bound to the dimer interface in the crystal structure of 6WUU (Rut et al., 2020), the docking studies were performed with dimer form. Similarly, PCB docked with the best score or binding energy of −9.8 Kcal/mol followed by Astaxanthin, (−9.3 Kcal/mol), β-carotene (−9.2 Kcal/mol), Daidzein (−8.9 Kcal/mol), Riboflavin (−8.5 Kcal/mol), and Genistein (−8.3 Kcal/mol). Eleven key active site amino acid residues (Asp 164, Tyr 264, Gln 269, Arg 166, Tyr 273, Glu 161, Tyr 268, Lys 157, Leu 162, Gly 266, and Ser 170) in chain A and 13 amino acid residues (Arg 166, Gln 174, Met 208, Glu 161, Glu 167, Cys 155, Lys 232, Met 206, Arg 183, Glu 203, Tyr 268, Tyr 273, and Thr 301) in chain B of SARS-CoV-2

TABLE 2 | Molecular docking results of food bioactive compounds with COVID-19 main protease (M^{pro}), papain-like protease (PL^{pro}).

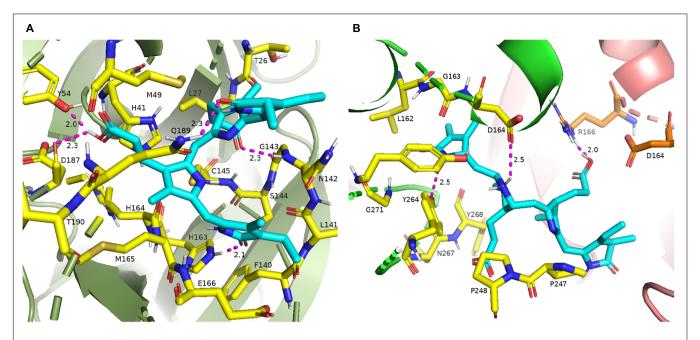| Source	Compounds	M^{pro}		PL^{pro}	
		Dock score	Polar contacts	Dock score	Polar contacts
Cyanobacteria	Phycocyanobilin	−8.6	Y54, G143, H163, D187, Q189	−9.8	D164 (A), R166 (B), Y264 (A)
Fruits, vegetables, seeds, and grains	Quercetin	−7.8	Y54, Q189	−8	R166 (B), Q269 (A)
Eggs, meat, fruits, and vegetables	Riboflavin	−7.9	E166, C145, H163, L141, S144	−8.5	R166 (A), Y264 (A), Y273 (A)
Grapes and berries	Cyanidin	−7.8	S144, H163	−7.9	E161 (A), Y268 (A)
Legumes	Daidzein	−7.8	T26, E166, Q192, T190	−8.9	K157 (A), D164 (A), R166 (B), Q174 (B)
Legumes	Genistein	−7.6	E166	−8.3	K157 (A), L162 (A), Q174 (B), M208 (B)
Green tea	Catechin	−7.3	L141, H163	−7.1	E161 (B), R166(A)
Grapes and berries skin	Resveratrol	−7	L141, H163, D187	−7.2	R166 (A), E167 (B), C155 (B)
Turmeric	Curcumin	−7	G143, S144, C145	−8	K157 (A), K232 (B), Y264 (A)
Microalgae	Astaxanthin	−7	None	−9.3	G266 (A), M206 (B)
Fruits and vegetables	β-carotene	−6.5	None	−9.2	None
Chili pepper	Capsaicin	−6.3	E166, T190, Q192	−6.5	K157 (A), M208 (B)
Ginger	Gingerol	−6.1	G143, S144, C145, H163, E166	−6.4	R183 (B), E203 (B), R183 (B)
Vanilla	Vanillin	−5	G143, S144, C145, H163, E166	−5.4	Y268 (B), Y273 (B), T301 (B)
Cloves	Eugenol	−4.9	L141, G143, S144, C145, H163	−5.6	S170 (A), C155 (B)
Thyme	Thymol	−4.8	None	−5.4	E203 (B)

FIGURE 1 | (A) 3-D binding pocket of SARS-CoV-2 M^pro with top model PCB (cyan color), surrounding active site amino acid residues (yellow color) within 3 Å; remaining residues are represented as a cartoon; **(B)** 3-D binding pocket of SARS-CoV-2 PL^pro with top model PCB (cyan color), surrounding active site amino acid residues (chain A, yellow color; chain B, orange color) within 3 Å; remaining residues are represented as a cartoon (chain A, green color; chain B, light pink color). Polar interactions are represented as magenta color.

PL^pro are involved in polar interactions at a distance of ≤ 3 Å with ligand phytochemical compounds. **Table 2** illustrates the specific polar contacts between phytochemical compounds and proteases. **Figure 1** shows a 3-D representation of the binding pocket of M^pro and PL^pro with top score model pose of PCB. The co-crystalized structure of native 6LU7-N3 and 6WUU-VIR250 complexes and polar contacts are represented in **Supplementary Figures 1a, 2a**. The docking validation studies reveal that both N3 peptide inhibitor and VIR250 bound exactly to the active site of 6LU7 and 6WUU, respectively. Superimposed redocked N3 on to the native co-crystallized N3 show a low RMSD of 1.82 Å was observed, whereas redocked VIR250 had a RMSD of 2.096 Å (**Supplementary Figures 1b, 2b**). These results show less variation in comparison with the native binding pose of ligands in co-crystallized form.

To evaluate the reliability of the molecular docking and stability of docked complexes, we conducted molecular dynamics simulations with a traditional force field (CHARMM36m), starting with the docking-generated pose of M^pro-ligand complexes with binding energy cutoff values of -7.6 Kcal/mol, PL^pro-ligand complexes with binding energy cut-off values of -8.0 Kcal/mol accompanying with a higher binding affinity toward M^pro. Root mean square deviation (RMSD) was measured to measure the structural conformation differences between the initial and final positions of proteins and ligands. **Table 3** depicts average ligand and protein RMSD and occupancy of major hydrogen bonds for food bioactive compounds in traditional MD simulations. The data show ligand RMSD values are in the range of 0.285 ± 0.090 to 1.743 ± 0.219, protein RMSD values are in the range of 1.370 ± 0.164 to 2.298 ± 0.353 in both M^pro and PL^pro

complexes. These lower RMSD values indicate greater stability of protein-ligand docked complexes.

In vitro Enzymatic Assay Studies to Screen Potent Phytochemical Inhibitor Compounds Against SARS-CoV-2 M^pro and PL^pro

To further validate the molecular docking and molecular dynamics studies, *in vitro* enzymatic studies were conducted. A positive control without the inhibitor compound in the reaction mixture, an inhibitor control that contains authentic inhibitors GC376 (for M^pro), GRL0617 (for PL^pro) were used in this study. The enzyme's relative activity in the presence of inhibitors was estimated by considering positive control activity as 100%. Based on *in silico* studies, we selected the top six phytochemicals (PCB, quercetin, riboflavin, cyanidin, daidzein, and genistein) with a binding energy cutoff value of -7.6 Kcal/mol for M^pro enzymatic assay studies. Initial screening results revealed that PCB had higher inhibitor activity followed by quercetin, genistein, cyanidin, and riboflavin ($p < 0.05$) (**Figure 2**). Further, the IC$_{50}$ value of top two compounds, PCB and quercetin, was determined, and the results show an effective IC$_{50}$ value of 71 μM for PCB (**Figure 3**) than quercetin (145 μM) (**Supplementary Figure 3**). For PL^pro, four compounds (Phycocyanobilin, Riboflavin, Genistein, and Quercetin) with a binding energy cutoff value of -8.0 Kcal/mol, accompanying higher inhibitor activity toward M^pro, were selected for the *in vitro* inhibitor activity assay (**Figure 2**). It was envisaged that PCB showed potent inhibitor activity compared to other

TABLE 3 | Average ligand and protein RMSD and occupancy of major hydrogen bonds for food bioactive compounds in traditional MD simulations.

Compound	Ligand-RMSD (Å)	Protein-RMSD (Å)	Major hydrogen bonds and its occupancy (%)
Mpro			
PCB	1.743 ± 0.219	1.720 ± 0.201	G143 (38.5), N119 (38.7), S46 (25.6), Y54 (12)
Quercetin	0.342 ± 0.104	1.372 ± 0.143	Y54 (18.7), E166 (10.9), S144 (4.5)
Cyanidin	0.832 ± 0.252	1.462 ± 0.207	H163 (34.6), H164 (13.5), G143 (6.7), N (5.9)
Daidzein	0.513 ± 0.145	1.407 ± 0.148	E166 (51.5), R188 (23.9), T190 (25.7), T26 (24.2), G143 (17.4)
Genistein	0.391 ± 0.088	1.370 ± 0.164	D187 (32), E166 (26.8), G143 (9.2), Q189 (4.2)
Riboflavin	1.131 ± 0.193	1.482 ± 0.297	H163 (33.9), N142 (24.7), E166 (15.9), R188 (10.2)
PLpro			
PCB	1.452 ± 0.125	2.226 ± 0.125	D164(C) (82.1), R166(C) (57.4), D164(A) (51.9), G271(A) (21.6)
Quercetin	0.875 ± 0.118	2.298 ± 0.353	E203(C) (54.5), E167(A) (27.6), S170(C) (22.7), M208(C) (21.4), Y171(A) (8.1), K157(A) (5.5),
Cyanidin	0.285 ± 0.090	1.988 ± 0.316	E203(C) (73.7), Y264(A) (15.1)
Daidzein	0.794 ± 0.088	2.02 ± 0.486	D164(A) (46.6), C155(A) (30.2), K157(A) (19.2), R166(A) (18.1)
Genistein	1.072 ± 0.196	1.864 ± 0.254	Q269(A) (51.9), M208(C) (21), Y171(A) (16.8), K157(A) (11.3)

Values in parentheses denotes hydrogen bonds occupancy (%).

compounds (**Figure 2**), with an IC$_{50}$ value of 62 μM (**Figure 3**). Overall, *in silico* docking and *in vitro* enzyme inhibitor activity data show PCB as a potent inhibitor against SARS-CoV-2 Mpro and PLpro.

In silico Insights of Broad-Spectrum Inhibitor Activity of PCB Against Mpro and PLpro

The broad-spectrum efficacy of PCB against CoVs was evaluated by molecular docking studies with available crystal PDB structure of various human and animal CoVs. **Table 4** shows the PDB identification code and top docking scores of PCB with Mpro and PLpro enzymes of human and animal CoVs. Due to the limitation on the availability of crystal PDB structures of PLpro, both dimer and monomeric forms were used in docking studies. For Mpro, docking scores are in the range of −8.3 to −9.3 Kcal/mol. PCB showed higher binding affinity with docking score (−9.3 Kcal/mol) for MERS Mpro followed by HCoV NL63 (−9.0 Kcal/mol) and IBV (−8.9 Kcal/mol). For PLpro, docking scores were in the range of −8.9 to −7.6 Kcal/mol. The results reveal that PCB had a higher binding affinity to the dimer form of PLpro enzymes than monomeric forms. When compared monomers only, PCB had best docking score for MERS-CoV (−8.5 Kcal/mol) followed by TGEV (−8.1 Kcal/mol) and SARS-CoV-2 (−8.0 Kcal/mol). **Supplementary Figures 4, 5** show polar contacts of PCB with binding pocket key amino acid residues of Mpro and PLpro enzymes of human and

animal CoVs. Surprisingly, the docking results suggest PCB as a promising broad-spectrum food bioactive inhibitor compound against CoVs proteases.

In silico Insights Into Inhibitor Activities of Other Phycobilins

Phycobilins are linear tetrapyrrole chromophore compounds found in certain photosynthetic organisms (cyanobacteria, red algae, glaucophytes, and some cryptomonads) and covalently linked to phycobiliproteins (Beale, 1993). Four types of phycobilins are identified: (i) phycoerythrobilin (PEB), (ii) phycourobilin (PUB), (iii) phycoviolobilin (PVB), and (iv) PCB. **Figure 4** represents the molecular structures of phycobilins. Based on the PCB results, the other phycobilin inhibitor activity against SARS-CoV-2 proteases via molecular docking approach was demonstrated and docking scores, polar contacts are given in **Table 5**. All phycobilins show strong binding affinity to key amino acids of Mpro and PLpro binding pockets. The docking scores were in the order of PUB (−8.7 Kcal/mol) > PCB (−8.6 Kcal/mol) > PEB (−8.2 Kcal/mol) > PVB (−8.2 Kcal/mol) for Mpro, whereas in the case of PLpro, the order was PCB (−9.8 Kcal/mol) = PEB (−9.8 Kcal/mol) > PUB (−9.6 Kcal/mol) > PVB (−9.5 Kcal/mol). Nine key binding pocket amino acids (Y54, L141, G143, S144, C145, H163, E166, D187, and Q189) of Mpro participated in polar contacts with phycobilins, and specific polar contacts of each phycobilin are shown in **Supplementary Figure 6**. Ten key binding pocket amino acids [D164 (A), Y264 (A), R166 (A), G266 (A), E161 (A), L162 (A), G271 (A), K232 (A), R166 (B), and T301 (B)] of PLpro participated in polar contacts with phycobilins; specific polar contacts are shown in **Supplementary Figure 6**.

DISCUSSION

Several SARS-CoV-2 mutants are spreading globally; most notably, mutants emerged in the United Kingdom (B.1.1.7), South Africa (B.1.351), and Brazil (P.1) (CDC, 2021). Hence, the efficacy of currently developed vaccines against these variants is questionable. The development of broad-spectrum antiviral drugs against existing viruses is an attractive approach that could provide first-line defense against emerging viral variants. The selection of highly conserved drug targets is an important step to develop broad-spectrum antiviral drugs. Sequence alignment analysis of SARS-CoV-2 and other CoVs (SARS-CoV and MERS) reveals that Mpro and PLpro are highly conserved, especially in the functional regions, which makes them potential targets for COVID-19 drug targets (Wu C. et al., 2020).

Several target-based *in silico* screening approaches were performed to find promising protease inhibitors among repurposed drugs, natural phytochemicals, and herbal medicinal compounds against COVID-19 (Amin et al., 2020; Wu C. et al., 2020; Xian et al., 2020). In this study, we focused on screening natural bioactive compounds for potential inhibitor activity against SARS-CoV-2 proteases. Amin et al. (2020) report the list of key amino acids involved in catalysis and substrate binding for Mpro (H41, C145, M49, G143, S144, H163, H164, M165, E166, L167, D187, R188, Q189, T190,

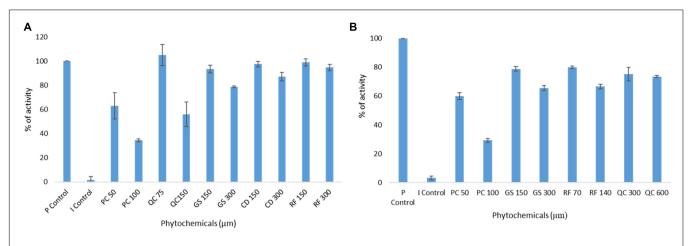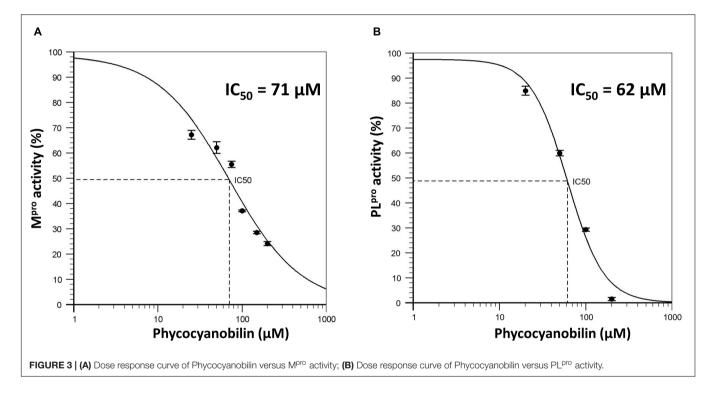**FIGURE 2 |** Initial screening of phytochemicals (selected based on docking score and our availability) by *in vitro* enzymatic assays; **(A)** Mpro assay; **(B)** PLpro assay; P control, positive control; I control, inhibitor control; PC, phycocyanobilin; QC, quercetin; GS, genistein; CD, cyaniding; RF, riboflavin.

FIGURE 3 | (A) Dose response curve of Phycocyanobilin versus M^{pro} activity; **(B)** Dose response curve of Phycocyanobilin versus PL^{pro} activity.

A191, and Q192) and PL^{pro} (C111, H272, D286, Y268, M208, P247, P248, T301, P248, Y264, N267, Q269, L162, C270, G271, and Y273). Our molecular docking results with natural compounds also show polar interactions in these specific substrate-binding regions for both proteases. Further *in vitro* validation studies found a good correlation between docking and enzymatic assay results. Both *in silico* and *in vitro* approaches show that PCB has strong inhibitor activity against both SARS-CoV-2 proteases. Shih et al. (2003) report direct antiviral activity of allophycocyanin against enterovirus 71 in human rhabdomyosarcoma cells and African green monkey kidney cells. In another study, El-Morsi et al. (2016) demonstrate the reduction of ΦX174 and MS2 by

extracted phycobiliproteins from cyanobacterium *Synechococcus cedrorum* Sauvageau.

Though numerous research studies report potential inhibitors with major emphasis on SARS-CoV-2, limited literature is available on broad-spectrum inhibitors against a wide range of CoVs, including human and animal CoVs. For instance, Sheahan et al. (2020) report broad-spectrum antiviral activity of ribonucleoside analog β-D-N4-hydroxycytidine (NHC; EIDD-1931) against SARS-CoV-2, SARS-CoV, MERS-CoV, and bat-CoVs. This study reports the broad-spectrum activity of natural phytochemical compound PCB against 11 CoVs (seven human CoVs and four animal CoVs). The computed physical properties of phycocyanobilin show a rotatable bond count of 10, hydrogen

TABLE 4 | Molecular docking results of phycocyanobilin with proteases of other pathogenic human and animal CoVs.

CoVs	PDB ID	Dock score	Polar contacts
M^{pro}			
SARS-CoV-1	1WOF	−8.5	Y54, N142, G143, S144, T190
MERS-CoV	5C3N	−9.3	H41 (2), Q167, K191 (2), Q195 (2)
MHV	6JIJ	−8.4	F138, H161, E164, Q187, Q190
TGEV	2AMP	−8.3	V26, H41, H162
FIPV	5EU8	−8.5	H41, T47, H162, H163, G167, Q191
IBV	2Q6F	−8.9	F46, G141, A142, C143, E187, Q190
HCoV 229 E	3DBP	−8.3	I140, H162, E165, G167
HCoV NL63	5DWY	−9	Y53, G142 (2), A143, H163, Q164
HCoV HKU1	3D23	−8.4	E166 (2), S168
PL^{pro}			
SARS-CoV-1 (dimer)	2FE8	−8.9	K158 (A), D165 (A), E168 (A), H172 (B)
SARS-CoV-1 (monomer)	2FE8	−7.6	L163, G164, Y269, T302
SARS-CoV-2 (monomer)	6LU7	−8.0	R166, G266
MERS-CoV (monomer)	4RNA	−8.5	D164, D165, G248, G277, Y279
TGEV (monomer)	3MP2	−8.1	D80, H153, Q180, G182, Y184
IBV (monomer)	4 × 2Z	−7.8	D150, F151 (2), S152, D153

TABLE 5 | Molecular docking results of other phycobilins with proteases of SARS-CoV-2.

Other phycobilins	Dock score	Polar contacts
M^{pro}		
Phycoerythrobilin	−8.2	L141, H163, E166, Q189 (2)
Phycourobilin	−8.7	G143, S144, C145, H163
Phycoviolobilin	−7.7	L141, G143, S144, C145, E166
PL^{pro}		
Phycoerythrobilin	−9.8	R166 (A), Y264 (A), T301 (B)
Phycourobilin	−9.6	R166 (A) (2), G266 (A)
Phycoviolobilin	−9.5	E161 (A), L162 (A), G271 (A), R166 (B) (2), K232 (A)

bond donor count of five, and hydrogen bond acceptor count of seven (National Center for Biotechnology Information (NCBI), 2020), which makes multiple hydrogen bond interactions between the compound and specific amino acid residues located at the active site of the pocket of the wide range of protease enzymes. Molecular docking studies indicated that propionic carboxyl and lactam ring carbonyl oxygens of PCB are involved in polar interactions with proteases' amino acid residues.

To investigate other structurally similar phycobilin (PEB, PUB, and PVB) inhibitor activity, we attempted molecular docking with SARS-CoV-2 proteases. The results reveal that, like PCB, all phycobilins show similar binding affinity toward M^{pro} and PL^{pro} of SARS-CoV-2. Besides this, potent therapeutic properties, such as peroxy radical scavenging, inhibition of cancer cell proliferation, and platelet aggregation are reported for phycobilins (Watanabe et al., 2014). Phycobilin compounds can be directly administered orally as phycobiliproteins

FIGURE 4 | Molecular structures of phycobilins; **(A)** PCB; **(B)** PEB; **(C)** PUB; **(D)** PVB.

(a complex of phycobilins and protein). For instance, when phycocyanin is administered orally to humans, it can be digested and free phycocyanobilin released in the gastrointestinal tract (Watanabe et al., 2014). Thus, noticed therapeutic properties of phycobiliproteins might reflect the effects of their phycobilins (chromophores).

In conclusion, by using *in silico* (molecular docking and MD simulations), *in vitro* enzymatic assay screenings, we discovered PCB as potent phytochemical inhibitors to M^{pro} and PL^{pro} proteases of SARS-CoV-2. Phycocyanobilin had IC_{50} values of 71 and 62 μM for SARS-CoV-2 M^{pro} and PL^{pro}, respectively. Further PCB docking studies with other CoVs Mpro and PLpro proteases revealed its broad-spectrum inhibitor activity. A similar binding affinity of other phycobilins (PEB, PUB, and PVB) to these proteases were observed. However, *in vitro* enzymatic studies with M^{pro} and PL^{pro} of other CoVs and *in vivo* studies on the inhibition of CoVs infectivity using human cells and animal models are needed. Further structure-guided development of phycobilin lead compounds could rapidly lead to discovering a single agent with clinical potential against existing and possible future emerging CoV-associated diseases.

DATA AVAILABILITY STATEMENT

The original contributions presented in the study are included in the article/**Supplementary Material**, further inquiries can be directed to the corresponding author/s.

AUTHOR CONTRIBUTIONS

BP: conceptualization, methodology, investigation, visualization, data curation, and writing original draft preparation. AP: conceptualization, supervision, writing, reviewing, and editing. CD: reviewing and editing. All authors contributed to the article and approved the submitted version.

SUPPLEMENTARY MATERIAL

The Supplementary Material for this article can be found online at: https://www.frontiersin.org/articles/10.3389/fmicb.2021.645713/full#supplementary-material

REFERENCES

Alfaraj, S. H., Al-Tawfiq, J. A., Assiri, A. Y., Alzahrani, N. A., Alanazi, A. A., and Memish, Z. A. (2019). Clinical predictors of mortality of Middle East Respiratory Syndrome Coronavirus (MERS-CoV) infection: a cohort study. *Travel Med. Infect. Dis.* 29, 48–50. doi: 10.1016/j.tmaid.2019.03.004

Amin, S. A., Banerjee, S., Ghosh, K., Gayen, S., and Jha, T. (2020). Protease targeted COVID-19 drug discovery and its challenges: insight into viral main protease (Mpro) and papain-like protease (PLpro) inhibitors. *Bioorg. Med. Chem.* 29:115860. doi: 10.1016/j.bmc.2020.115860

Bachmetov, L., Gal-Tanamy, M., Shapira, A., Vorobeychik, M., Giterman-Galam, T., Sathiyamoorthy, P., et al. (2012). Suppression of hepatitis C virus by the flavonoid quercetin is mediated by inhibition of NS3 protease activity. *J. Viral Hepat.* 19, e81–e88.

Beale, S. I. (1993). Biosynthesis of phycobilins. *Chem. Rev.* 93, 785–802. doi: 10.1021/cr00018a008

Bekerman, E., and Einav, S. (2015). Combating emerging viral threats. *Science* 348, 282–283. doi: 10.1126/science.aaa3778

Benencia, F., and Courreges, M. C. (2000). In vitro and in vivo activity of eugenol on human herpesvirus. *Phytother. Res.* 14, 495–500. doi: 10.1002/1099-1573(200011)14:7<495::aid-ptr650>3.0.co;2-8

Bermingham, A., Chand, M. A., Brown, C. S., Aarons, E., Tong, C., Langrish, C., et al. (2012). Severe respiratory illness caused by a novel coronavirus, in a patient transferred to the United Kingdom from the Middle East, September 2012. *Eurosurveillance* 17:20290.

Carmichael, L. E. (1999). Canine viral vaccines at a turning point—a personal perspective. *Adv. Vet. Med.* 41, 289–307. doi: 10.1016/s0065-3519(99)80022-6

Cavanagh, D. (2007). Coronavirus avian infectious bronchitis virus. *Vet. Res.* 38, 281–297. doi: 10.1051/vetres:2006055

CDC (2021). *Emerging SARS-CoV-2 Variants*. Available online at: https://www.cdc.gov/coronavirus/2019-ncov/more/science-and-research/scientific-brief-emerging-variants.html (accessed January 28, 2021).

Chen, Y. H., Chang, G. K., Kuo, S. M., Huang, S. Y., Hu, I. C., Lo, Y. L., et al. (2016). Well-tolerated Spirulina extract inhibits influenza virus replication and reduces virus-induced mortality. *Sci. Rep.* 6:24253.

Cho, N. J., and Glenn, J. S. (2020). Materials science approaches in the development of broad-spectrum antiviral therapies. *Nat. Mater.* 19, 813–816. doi: 10.1038/s41563-020-0698-4

Cleri, D. J., Ricketti, A. J., and Vernaleo, J. R. (2010). Severe acute respiratory syndrome (SARS). *Infect. Dis. Clin.* 24, 175–202.

De Clercq, E. (2004). Antivirals and antiviral strategies. *Nat. Rev. Microbiol.* 2, 704–720. doi: 10.1038/nrmicro975

Drosten, C., Günther, S., Preiser, W., van der Werf, S., Brodt, H. R., Becker, S., et al. (2003). Identification of a novel coronavirus in patients with severe acute respiratory syndrome. *N. Engl. J. Med.* 348, 1967–1976.

El-Morsi, A. A., Abd El-Hamid, M. I., and Abd El-Fatah, W. M. (2016). Anti-hepatitis viruses of phycobiliprotiens aqueous extract of the cyanobacterium *Synechococcu scedrorum* Sauvageau using bacteriophages MS-2/ΦX-174 as model systems. *J. Environ. Sci.* 45, 119–130.

Fauci, A. S., and Morens, D. M. (2016). Zika virus in the Americas—yet another arbovirus threat. *N. Engl. J. Med.* 374, 601–604. doi: 10.1056/nejmp1600297

Feller, S. E., Zhang, Y., Pastor, R. W., and Brooks, B. R. (1995). Constant pressure molecular dynamics simulation: the Langevin piston method. *J. Chem. Phys.* 103, 4613–4621. doi: 10.1063/1.470648

Ghildiyal, R., Prakash, V., Chaudhary, V. K., Gupta, V., and Gabrani, R. (2020). "Phytochemicals as antiviral agents: recent updates," in *Plant-Derived Bioactives*, ed. M. Swamy (Singapore: Springer), 279–295. doi: 10.1007/978-981-15-1761-7_12

Hafiz, T. A., Mubaraki, M., Dkhil, M., and Al-Quraishy, S. (2017). Antiviral activities of *Capsicum annuum* methanolic extract against herpes simplex virus 1 and 2. *Pak. J. Zool.* 49, 251–255. doi: 10.17582/journal.pjz/2017.49.1.251.255

Hamre, D., and Procknow, J. J. (1966). A new virus isolated from the human respiratory tract. *Proc. Soc. Exp. Biol. Med.* 121, 190–193. doi: 10.3181/00379727-121-30734

Hangartner, L., Zinkernagel, R. M., and Hengartner, H. (2006). Antiviral antibody responses: the two extremes of a wide spectrum. *Nat. Rev. Immunol.* 6, 231–243. doi: 10.1038/nri1783

Hariono, M., Abdullah, N., Damodaran, K. V., Kamarulzaman, E. E., Mohamed, N., Hassan, S. S., et al. (2016). Potential new H1N1 neuraminidase inhibitors from ferulic acid and vanillin: molecular modelling, synthesis and in vitro assay. *Sci. Rep.* 6:38692.

Humphrey, W., Dalke, A., and Schulten, K. (1996). VMD: visual molecular dynamics. *J. Mol. Graph.* 14, 33–38. doi: 10.1016/0263-7855(96)00018-5

Jamison, J. M., Krabill, K., Hatwalkar, A., Jamison, E., and Tsai, C. C. (1990). Potentiation of the antiviral activity of poly r (AU) by xanthene dyes. *Cell Biol. Int. Rep.* 14, 1075–1084. doi: 10.1016/0309-1651(90)90015-q

Jo, S., Kim, T., Iyer, V. G., and Im, W. (2008). CHARMM-GUI: a web-based graphical user interface for CHARMM. *J. Comput. Chem.* 29, 1859–1865. doi: 10.1002/jcc.20945

Kannan, S., and Kolandaivel, P. (2018). The inhibitory performance of flavonoid cyanidin-3-sambubiocide against H274Y mutation in H1N1 influenza virus. *J. Biomol. Struct. Dyn.* 36, 4255–4269. doi: 10.1080/07391102.2017.1413422

Lai, W. L., Chuang, H. S., Lee, M. H., Wei, C. L., Lin, C. F., and Tsai, Y. C. (2012). Inhibition of herpes simplex virus type 1 by thymol-related monoterpenoids. *Planta Med.* 78, 1636–1638. doi: 10.1055/s-0032-1315208

LeCher, J. C., Diep, N., Krug, P. W., and Hilliard, J. K. (2019). Genistein has antiviral activity against herpes b virus and acts synergistically with antiviral treatments to reduce effective dose. *Viruses* 11:499. doi: 10.3390/v11060499

Lin, S. C., Ho, C. T., Chuo, W. H., Li, S., Wang, T. T., and Lin, C. C. (2017). Effective inhibition of MERS-CoV infection by resveratrol. *BMC Infect. Dis.* 17:144. doi: 10.1186/s12879-017-2253-8

Liu, S., and Kong, X. (2004). A new genotype of nephropathogenic infectious bronchitis virus circulating in vaccinated and non-vaccinated flocks in China. *Avian Pathol.* 33, 321–327. doi: 10.1080/0307945042000220697

Mani, J. S., Johnson, J. B., Steel, J. C., Broszczak, D. A., Neilsen, P. M., Walsh, K. B., et al. (2020). Natural product-derived phytochemicals as potential agents against coronaviruses: a review. *Virus Res.* 284:197989. doi: 10.1016/j.virusres.2020.197989

McIntosh, K., Becker, W. B., and Chanock, R. M. (1967). Growth in suckling-mouse brain of "IBV-like" viruses from patients with upper respiratory tract disease. *Proc. Natl. Acad. Sci. U.S.A.* 58, 2268–2273. doi: 10.1073/pnas.58.6.2268

National Center for Biotechnology Information (NCBI) (2020). *PubChem Compound Summary for CID 365902, Phycocyanobilin*. Available online at: https://pubchem.ncbi.nlm.nih.gov/compound/Phycocyanobilin (accessed November 9, 2020)

O'Boyle, N. M., Banck, M., James, C. A., Morley, C., Vandermeersch, T., and Hutchison, G. R. (2011). Open Babel: an open chemical toolbox. *J. Cheminform.* 3:33.

Odend'hal, S. (2012). Porcine transmissible gastroenteritis virus. *Geogr. Distrib. Anim. Viral Dis.* 1983, 329–331. doi: 10.1016/b978-0-12-524180-9.50089-3

Park, S., Sestak, K., Hodgins, D. C., Shoup, D. I., Ward, L. A., Jackwood, D. J., et al. (1998). Immune response of sows vaccinated with attenuated transmissible gastroenteritis virus (TGEV) and recombinant TGEV spike protein vaccines and protection of their suckling pigs against virulent TGEV challenge exposure. *Am. J. Vet. Res.* 59, 1002–1008.

Paules, C. I., Marston, H. D., and Fauci, A. S. (2020). Coronavirus infections—more than just the common cold. *JAMA* 323, 707–708. doi: 10.1001/jama.2020.0757

Pedersen, N. C. (2009). A review of feline infectious peritonitis virus infection: 1963–2008. *J. Feline Med. Surg.* 11, 225–258. doi: 10.1016/j.jfms.2008.09.008

Phillips, J. C., Braun, R., Wang, W., Gumbart, J., Tajkhorshid, E., Villa, E., et al. (2005). Scalable molecular dynamics with NAMD. *J. Comput. Chem.* 26, 1781–1802.

Pratelli, A. (2006). Genetic evolution of canine coronavirus and recent advances in prophylaxis. *Vet. Res.* 37, 191–200. doi: 10.1051/vetres:2005053

Rut, W., Lv, Z., Zmudzinski, M., Patchett, S., Nayak, D., Snipas, S. J., et al. (2020). Activity profiling and crystal structures of inhibitor-bound SARS-CoV-2 papain-like protease: a framework for anti–COVID-19 drug design. *Sci. Adv.* 6:eabd4596. doi: 10.1126/sciadv.abd4596

San Chang, J., Wang, K. C., Yeh, C. F., Shieh, D. E., and Chiang, L. C. (2013). Fresh ginger (*Zingiber officinale*) has anti-viral activity against human respiratory syncytial virus in human respiratory tract cell lines. *J. Ethnopharmacol.* 145, 146–151. doi: 10.1016/j.jep.2012.10.043

Santoyo, S., Jaime, L., Plaza, M., Herrero, M., Rodriguez-Meizoso, I., Ibañez, E., et al. (2012). Antiviral compounds obtained from microalgae commonly used as carotenoid sources. *J. Appl. Phycol.* 24, 731–741. doi: 10.1007/s10811-011-9692-1

Sheahan, T. P., Sims, A. C., Zhou, S., Graham, R. L., Pruijssers, A. J., Agostini, M. L., et al. (2020). An orally bioavailable broad-spectrum antiviral inhibits SARS-CoV-2 in human airway epithelial cell cultures and multiple coronaviruses in mice. *Sci. Transl. Med.* 12:eabb5883. doi: 10.1126/scitranslmed.abb5883

Shih, S. R., Tsai, K. N., Li, Y. S., Chueh, C. C., and Chan, E. C. (2003). Inhibition of enterovirus 71-induced apoptosis by allophycocyanin isolated from a blue-green alga *Spirulina platensis*. *J. Med. Virol.* 70, 119–125.

Song, J. M., Lee, K. H., and Seong, B. L. (2005). Antiviral effect of catechins in green tea on influenza virus. *Antiviral Res.* 68, 66–74. doi: 10.1016/j.antiviral.2005.06.010

Totura, A. L., and Bavari, S. (2019). Broad-spectrum coronavirus antiviral drug discovery. *Expert Opin. Drug Discov.* 14, 397–412. doi: 10.1080/17460441.2019.1581171

Trott, O., and Olson, A. J. (2010). AutoDock Vina: improving the speed and accuracy of docking with a new scoring function, efficient optimization, and multithreading. *J. Comput. Chem.* 31, 455–461.

van der Hoek, L., Pyrc, K., Jebbink, M. F., Vermeulen-Oost, W., Berkhout, R. J., Wolthers, K. C., et al. (2004). Identification of a new human coronavirus. *Nat. Med.* 10, 368–373.

Watanabe, F., Yabuta, Y., and Bito, T. (2014). "Tetrapyrrole compounds of cyanobacteria," in *Studies in Natural Products Chemistry*, Vol. 42, ed. Atta-ur-Rahman (Amsterdam: Elsevier), 341–351. doi: 10.1016/b978-0-444-63281-4.00011-2

Woo, P. C., Huang, Y., Lau, S. K., and Yuen, K. Y. (2010). Coronavirus genomics and bioinformatics analysis. *Viruses* 2, 1804–1820. doi: 10.3390/v2081803

Woo, P. C., Lau, S. K., Chu, C. M., Chan, K. H., Tsoi, H. W., Huang, Y., et al. (2005). Characterization and complete genome sequence of a novel coronavirus, coronavirus HKU1, from patients with pneumonia. *J. Virol.* 79, 884–895. doi: 10.1128/jvi.79.2.884-895.2005

World Health Organization (WHO) (2003). *Consensus Document on the Epidemiology of Severe Acute Respiratory Syndrome (SARS)* (No. WHO/CDS/CSR/GAR/2003.11). Geneva: World Health Organization.

World Health Organization (WHO) (2020). *Coronavirus Disease 2019 (COVID-19)*. Available online at: https://www.who.int/docs/default-source/coronaviruse/situation-reports/20201012-weekly-epi-update-9.pdf (accessed October 12, 2020).

Wu, C., Liu, Y., Yang, Y., Zhang, P., Zhong, W., Wang, Y., et al. (2020). Analysis of therapeutic targets for SARS-CoV-2 and discovery of potential drugs by computational methods. *Acta Pharm. Sin. B* 10, 766–788. doi: 10.1016/j.apsb.2020.02.008

Wu, F., Zhao, S., Yu, B., Chen, Y. M., Wang, W., Song, Z. G., et al. (2020). A new coronavirus associated with human respiratory disease in China. *Nature* 579, 265–269.

Xian, Y., Zhang, J., Bian, Z., Zhou, H., Zhang, Z., Lin, Z., et al. (2020). Bioactive natural compounds against human coronaviruses: a review and perspective. *Acta Pharma. Sin. B* 10, 1163–1174. doi: 10.1016/j.apsb.2020.06.002

Zandi, K., Ramedani, E., Mohammadi, K., Tajbakhsh, S., Deilami, I., Rastian, Z., et al. (2010). Evaluation of antiviral activities of curcumin derivatives against HSV-1 in Vero cell line. *Nat. Prod. Commun.* 5, 1935–1938.

Zandi, K., Teoh, B. T., Sam, S. S., Wong, P. F., Mustafa, M. R., and AbuBakar, S. (2011). Antiviral activity of four types of bioflavonoid against dengue virus type-2. *Virol. J.* 8:560. doi: 10.1186/1743-422x-8-560

Zhang, L., Lin, D., Sun, X., Curth, U., Drosten, C., Sauerhering, L., et al. (2020). Crystal structure of SARS-CoV-2 main protease provides a basis for design of improved α-ketoamide inhibitors. *Science* 368, 409–412. doi: 10.1126/science.abb3405

Zhu, L., George, S., Schmidt, M. F., Al-Gharabli, S. I., Rademann, J., and Hilgenfeld, R. (2011). Peptide aldehyde inhibitors challenge the substrate specificity of the SARS-coronavirus main protease. *Antiviral Res.* 92, 204–212. doi: 10.1016/j.antiviral.2011.08.001